THE UNIVERSITY OF KANSAS CENTER FOR RESEARCH, INC.
2291 Irving Hill Drive—Campus West
Lawrence, Kansas 66045

RSL Remote Sensing Laboratory

The University of Kansas Center for Research, Inc.
2291 Irving Hill Drive-Campus West, Lawrence, Kansas 66045

Telephone: (913) 864-4832

NOSS-SCAT WIND DIRECTION ALIAS REMOVAL

K. Sam Shanmugan
V. Narayanan
J. Stiles

RSL TR 515-1
Final Report

January 1982

Remote Sensing Laboratory
University of Kansas Center for Research, Inc.
Lawrence, Kansas 66045

Supported By:

NASA Langley Research Center, Hampton, Virginia
Under Grant NASA-NAG-1-117

ABSTRACT

This report summarizes the results of using automated algorithms for removing aliases in NOSS-SCAT data. The algorithms used for alias removal consist of histogram analysis, local averaging and curve fitting. The histogram analysis is used to determine the degree of homogeneity of the wind field defined by the largest probability alias vector at each grid point. Depending on the degree of homogeneity, either a local averaging technique or a curve fitting technique is used to find a "preferred" wind direction at each grid location. The alias directions are compared with the preferred direction at each grid location and one of the multiple aliases is chosen as the true direction based on its closeness to the preferred direction and its probability.

The alias removal algorithms were applied to a number of simulated NOSS-SCAT data sets. The alias removal algorithms produced correct wind vectors with an accuracy of over 95%. This compares with about 80 to 85% of the grid points at which the alias with the largest probability is also the correct solution.

TABLE OF CONTENTS

LIST OF FIGURES

LIST OF TABLES

1.0 INTRODUCTION

The major steps in the alias removal procedure are shown in Figure 1. The raw data is rearranged first into 10x10x26 arrays where each array contains all the data from a processing area covering 10 grid locations along-track and 10 grid locations across-track. The 10x10 processing area size was determined from consideration of an area small enough in size to provide some degree of homogeneity and large enough to contain enough information about underlying streamline patterns. The streamline patterns were determined using the alias direction with the largest probability at each grid location. (Most of the processing was done on the array of largest probability aliases, i.e., the primary alias at each location.)

The primary alias wind field over the processing area was used to compare histograms of wind directions, wind spread and wind speed gradient. For each histogram, the mean, standard deviation and the entropy were also calculated. The standard deviation and entropy were used to determine the degree of homogeneity or uniformity of the wind field over a given area. If standard deviation and entropy were small, then the local average value of the wind direction was used to aid in alias removal. At locations where the local standard deviation was large, then the average value of the primary alias directions over the entire processing area was used for alias removal.

Higher values of standard deviation and entropy indicates the presence of a nonuniform wind field over the processing area produced by convergent set of streamlines, circulation patterns near lows, col point, or a frontal zone. In these cases a least square curve fitting algorithm is used to fit a streamline pattern to the primary alias wind

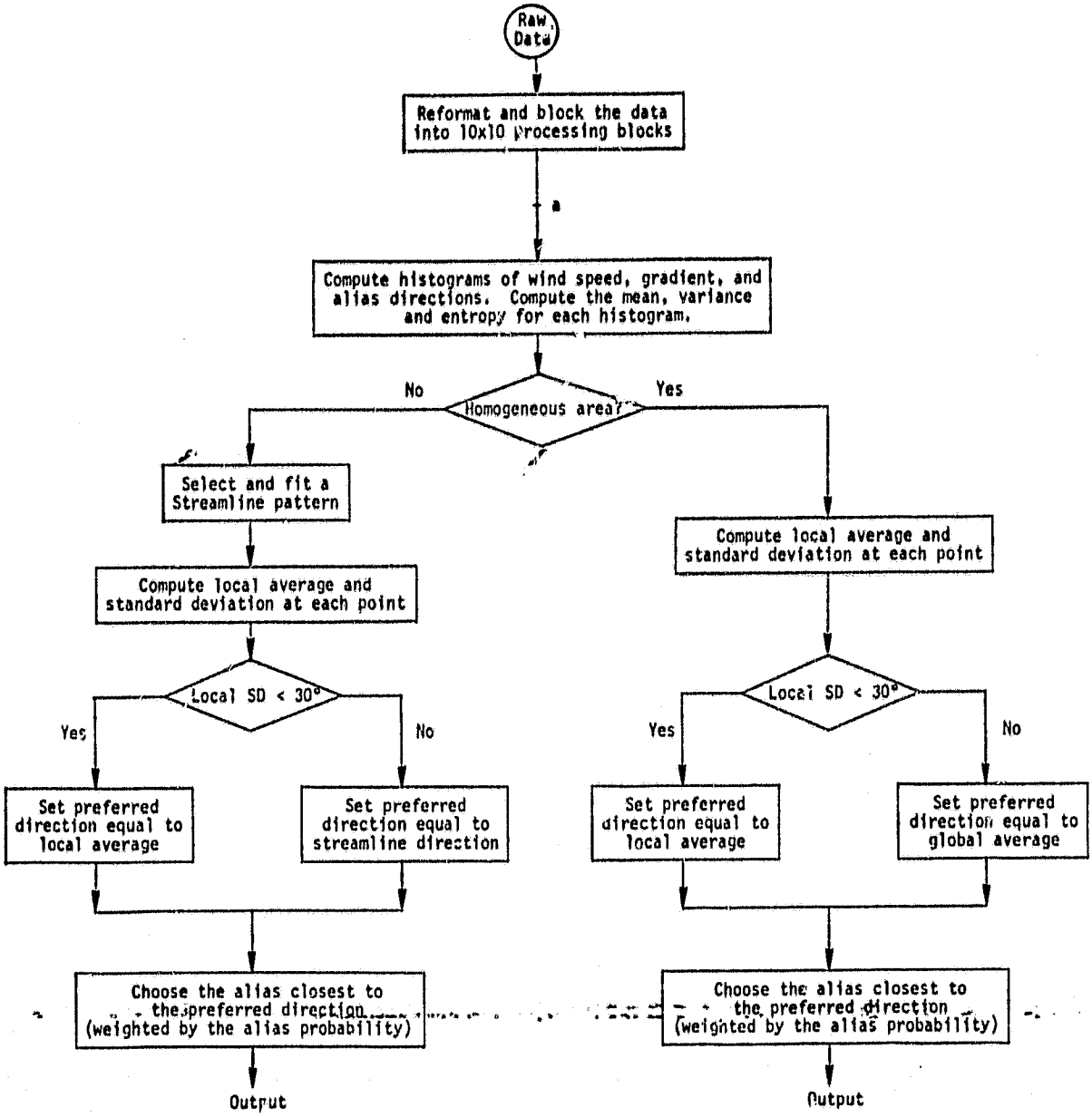

Figure 1. Major steps of the alias removal algorithm.

field. The streamline pattern establishes a preferred direction at each point in the context of the directions at other points within the processing area.

Given a context-derived preferred wind direction at a grid location, a choice is then made as to which one of the multiple solutions is the correct solution at a given location. This choice is made on the basis of the difference between an alias direction and the preferred direction, and the probability of the alias direction. The final output of the algorithm is a unique wind direction for each grid location. The accuracy of the algorithm is evaluated by counting the number of locations at which the algorithm selects, as its output, the alias direction closest to the true wind direction.

The alias removal algorithm was used to process a simulated NOSS-SCAT data set (Rev 0825 among others). Histogram analysis indicated that the left track contained slowly changing wind fields and the local averaging technique was used for alias removal. This algorithm selected the correct alias, i.e., the alias closest to the true direction, at 448 grid points out of 449 points processed. The largest probability alias was the correct alias at 436 out of 449 points.

The right track of the data set contained two lows and a col point. These locations were easily identified using the histogram analysis. The curve fitting approach was tested in the areas containing the lows. The alias removal algorithm selected the correct aliases at 133 points out of 143 points processed. The largest probability alias was the correct alias at 114 out of 143 points.

Similar results were obtained for a number of other simulated NOSS-SCAT data sets. Details of the alias removal algorithm are given in the following sections of this report.

2.0 REFORMATTING OF THE DATA SET

The first operation that was performed was the reformatting of the data. The data for the two tracks were separated and each track was broken up into 10x10 blocks. There was an overlap of 5 rows between each of these blocks. The size of the measurement vector for each bin was reduced from 37 in the original tape to 26 in the reformatted version. The components of the measurement vector chosen were:

1. column coordinate of the bin,
2. row coordinate of the bin,
3. average latitude of the measurements in the bin,
4. average longitude of the measurements in the bin,
5. average x coordinate of the measurements,
6. average y coordinate of the measurements,
7. wind speed from the original (true) wind field data,
8. wind direction measured from north from the original (true) wind field data,
9. average wind speed (average of speed associated with each alias),
10. number of aliases in the bin,

for each of the four aliases:

a. alias probability,

b. estimated speed for this alias,

c. estimated direction for this alias,

d. magnitude of the residual.

3.0 HISTOGRAM ANALYSES

A simple statistical analysis of each block was performed. The variables chosen were:

(1) average wind speed,

(2) wind direction associated with the largest alias probability,

(3) average wind speed gradient.

Each of the above variables was characterized by the following statistical descriptors:

(a) mean,

(b) standard deviation,

(c) entropy,

(d) histogram,

(e) minimum, maximum and their locations.

A weighted histogram was used for wind direction, i.e., the count in a cell, instead of being incremented by 1 is incremented by the probability. The formulae used to calculate mean and standard deviation of the wind directions are described in Appendix I. The gradient operator used on the average speed was a "Max Gradient" and is described in Appendix II. The average speed (and hence the gradient) varied from 0 m/s to 24 m/s. To construct the histogram this range was divided into 16 cells. The wind direction range (0° to 360°) was also divided into 16 cells. As a consequence the entropy varied from 0 to $\sum_{i=1}^{16} \frac{1}{16} \log_2 16 = 4$. An entropy of 4 is indicative of an uniform distribution, and 0 is indicative of a histogram that consists of one nonempty cell.

The true and aliased wind fields over the processing area are shown in Figures 2.a and 2.b, and a summary of the statistical para-

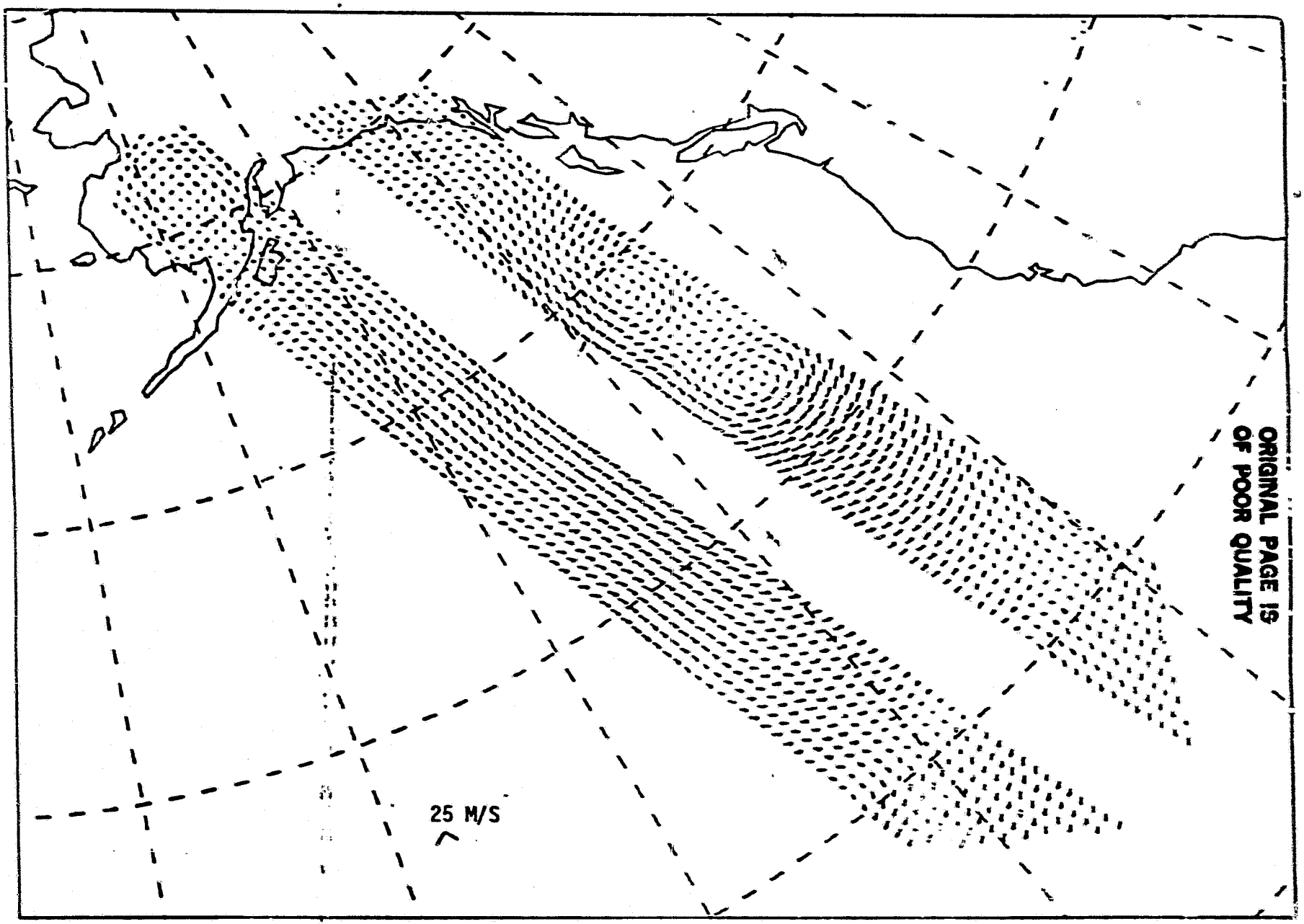

SURFACE TRUTH WIND ---- WIND FLOW IN DIRECTION OF ARROWS

Figure 2.a

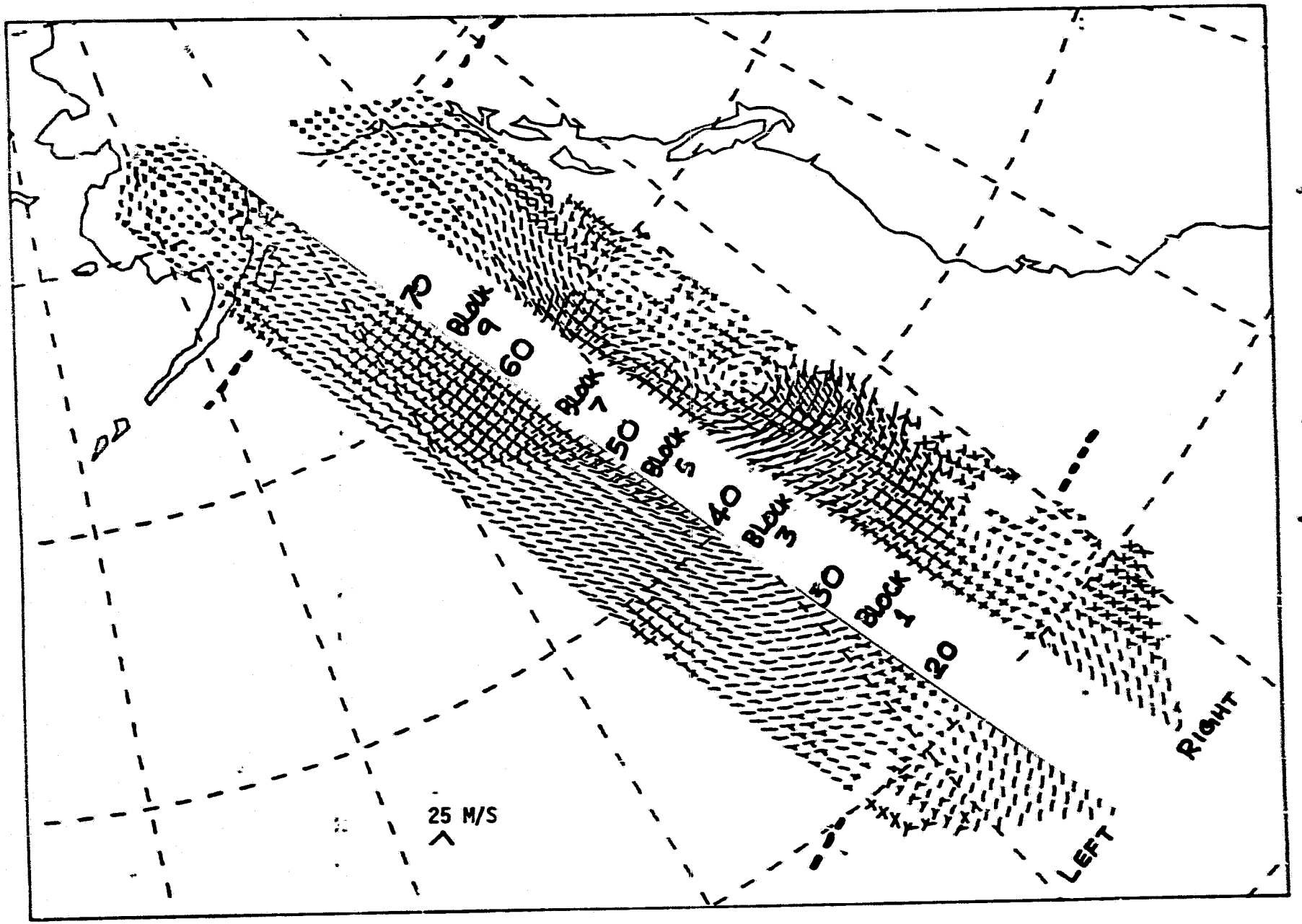

SEA CHICKEN PLOT-WIND FLOW IN DIRECTION AWAY FROM CENTER

Figure 2.b

meters of data within 10x10 processing areas are shown in Tables 1.a and 1.b. Specific examples of aliased wind fields, the histograms and the values of mean, variance and entropy are given for two processing areas in Figures 3.a and 3.b. The examples show clearly that the histogram analysis indeed provides an indication of whether the wind field is uniform or nonuniform over the processing area. Entries in Table 1.b, for example, show that the entropies of the wind speed gradient and wind direction are significantly larger in processing areas 4-8 which contain the lows. Entropies lower than 2 seem to indicate uniform wind fields, while higher values correspond to lows, col points, etc. This information is used in the next step of the alias removal algorithms.

Block #	Average Wind Speed			Wind Speed Gradient		Wind Direction Associated With Largest Alias Probability		
	Avg.	σ	Entropy	Avg.	Entropy	Avg.	σ	Entropy
1	8.1	1.8	2.0	1.2	0.9	282.5	46	2.0
2	9.5	1	1.5	0.8	0.3	298.5	35	1.6
3	10.7	2.1	2.6	1.5	1.0	318.3	29	1.7
4	13.4	2.5	2.5	1.5	1.0	335.0	27	1.0
5	14.0	1.7	2.3	1.2	0.8	320.8	24	0.9
6	12.1	2.05	2.5	1.6	1.0	321.4	18	1.1
7	10.6	1.7	2.2	1.3	1.0	331	24	1.5
8	10.3	1.4	1.9	1.1	0.8	348	24	0.9
9	9.3	1.4	1.7	1.0	0.4	350	26	0.8
10	7.8	.8	1.3	0.6	0.2	335	27	1.3
Mean=	10.58	1.65	2.05	1.18	.74	324.05	28	1.28

Table 1.a

Some Statistical Quantities for the Left Track

Block #	Average Wind Speed			Wind Speed Gradient		Wind Direction Associated With Largest Alias Probability		
	Avg.	σ	Entropy	Avg.	Entropy	Avg.	σ	Entropy
1	7.1	4	2.4	2.5	2.0	263	50	2.2
2	10.5	3	1.8	1.0	0.8	263	38	1.7
3	13.8	4.1	2.8	2.2	1.8	265	31	2.0
4	13.8	5.5	3.4	4.3	2.3	251	58	3.0
5	9.4	5.1	3.4	4.1	2.4	360	86	3.7
6	7.4	3.8	2.9	3.1	2.0	351	78	3.6
7	8	4.0	2.9	3.4	2.1	342	73	3.4
8	9.4	3.5	2.9	2.7	2.0	23	52	3.1
9	9.3	2.1	2.2	1.7	1.4	25	40	2.1
10	6.4	2.4	2.4	1.5	1.1	351	60	2.9
Mean=	9.51	3.75	2.71	2.65	1.79	321.4	56.6	2.77

Table 1.b

Some Statistical Quantities for the Right Track

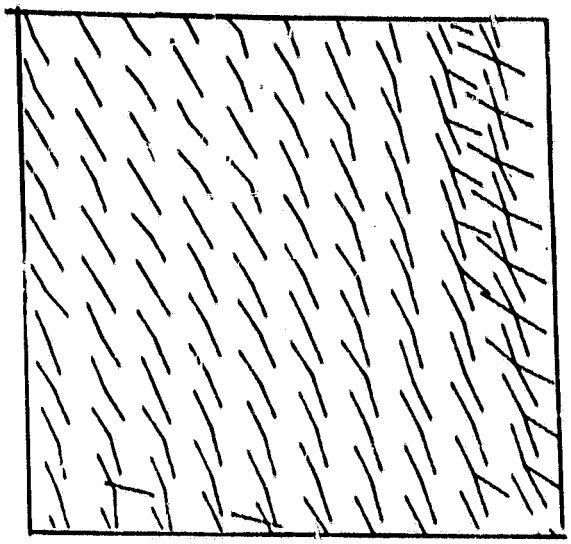

Aliased
Wind Field

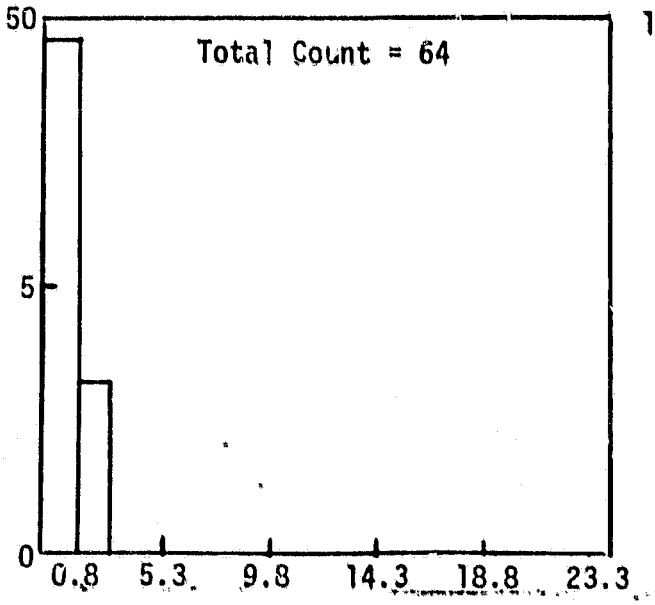

Histogram of Wind Speed Gradient

Mean = 1.2 m/s
Standard Deviation = 0.5 m/s
Entropy = 0.8

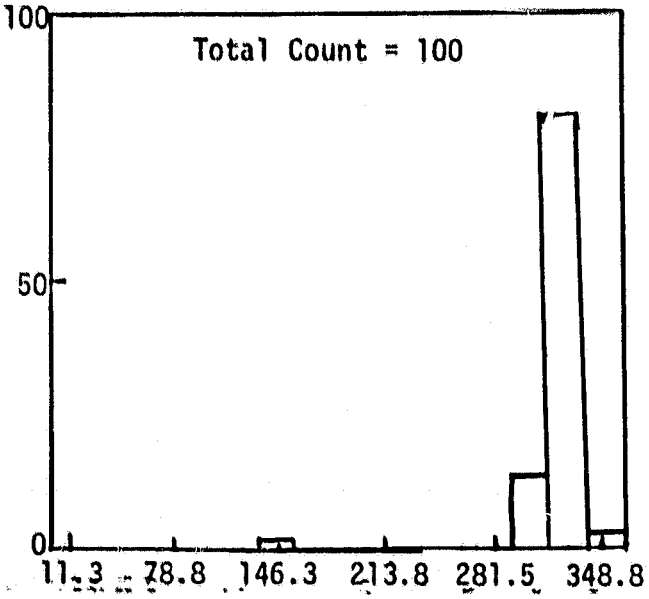

Histogram of Wind Direction With
Largest Alias Probability

Mean = 320.8°
Standard Deviation = 24.2°
Entropy = 0.9

Figure 3.a. Example of histograms (left track).

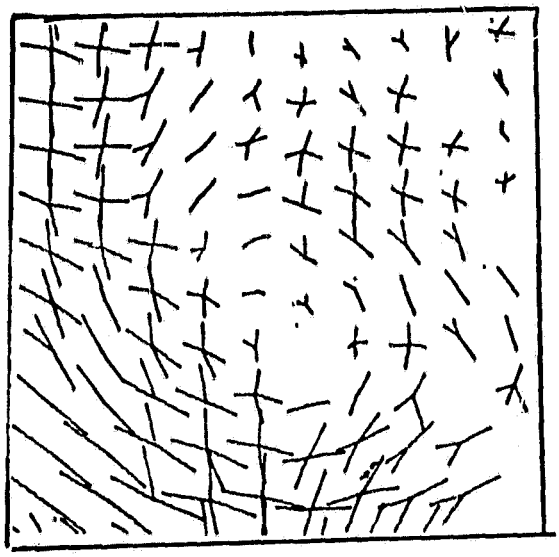

Aliased
Wind Field

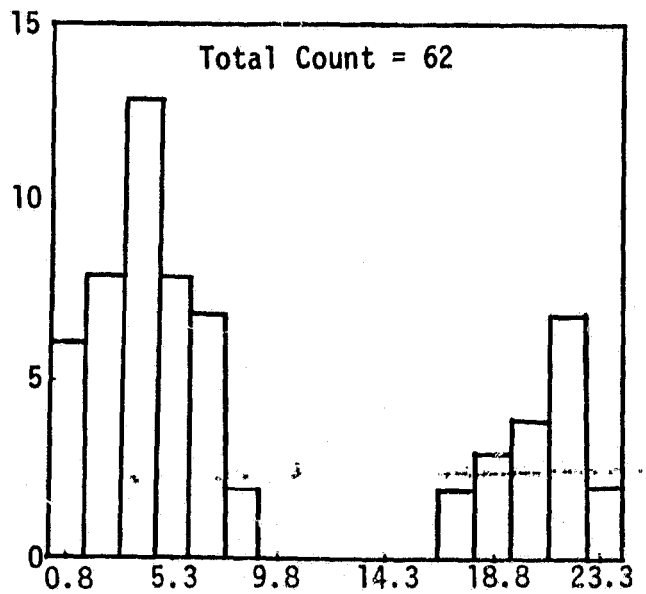

Histogram of Wind Speed

Mean = 9.4 m/s
Standard Deviation = 5.1 m/s
Entropy = 3.4

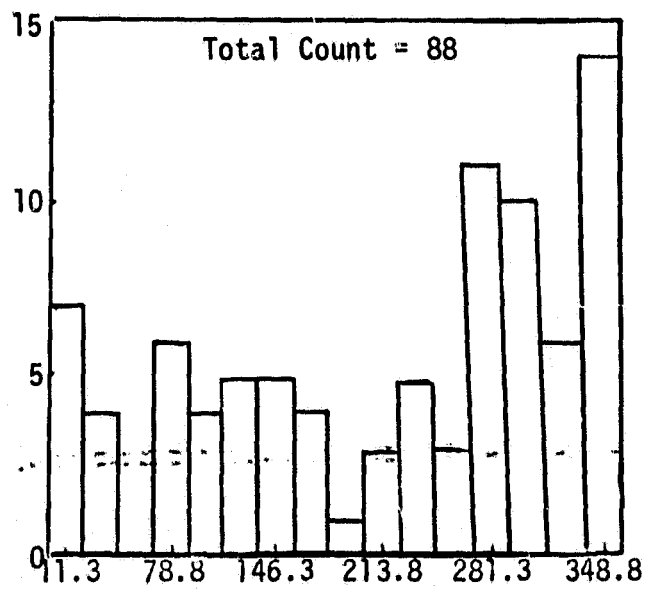

Histogram of Wind Direction With
Largest Alias Probability

Mean = 358.2°
Standard Deviation = 88.3°
Entropy = 3.7

Figure 3.b. Example of histograms (right track).

4.0 ALIAS REMOVAL BASED ON AVERAGES

The following conclusions can be drawn from the values of the statistical parameters for the processing areas in the left track shown in Table 1.a:

(a) There is not much change in wind direction from one block to another. The average wind direction for the whole track is 34.05° with a standard deviation of 28°.

(b) The entropy associated with direction is also small, (1.28 on an average) indicating a 'spiky' rather than an uniform probability distribution.

(c) The average wind speed gradient is small with an entropy close to zero. So the rate at which the average speed changes is low. This coupled with the fact that the wind direction varies slowly with a relatively small standard deviation (28°) is indicative of the absence of cyclonic, anticyclonic or other such patterns.

Because of the gradual changes in the wind field along the left track it would appear that simple local averaging could be used for alias removal. So, a 3x3 window was chosen and the averaging was done over the 9 entries in the window. (Since we are working with angles, care should be taken to follow the procedure outlined in Appendix I.) The direction associated with the largest alias probability was the variable we chose to work with. The local average at each point was taken as the preferred wind direction and the alias closest to the preferred direction was selected as the correct alias according to the following algorithm:

$$k = \max_i \left\{ \frac{1}{d_i r_i^{\beta}} \right\}, \qquad (1)$$

Alias direction selected = θ_k,

where: d_i = angular difference between the preferred direction (local average) and the ith alias direction θ_i,

r_i = residue corresponding to θ_i,

β = a positive constant, $0 < \beta < 1$.

The figure of merit used to measure the performance of the alias removal algorithm was the comparison between the 'number of agreements between the alias closest to true direction and the alias closest to average direction' on the one hand and 'the number of agreements between the alias closest to true direction and the alias with the largest probability' on the other.

Local averaging by itself did not clean up the track satisfactorily, because there are cells where the direction with the largest alias probability was not very close to the true direction and there were cells for which no measurement was available. This resulted in the wrong alias being chosen. And an error in one cell affects the average of the neighboring cells.

To rectify this problem, for each window not only is the local mean calculated but also the local standard deviation (σ), and if the standard deviation is above a certain value α then instead of the local average the average of the whole block (global average) is used as the average for that cell (see Figure 4a). This experiment was carried out for $\alpha = 5°, 20°, 30°, 45°, 60°$. The performance was the same for all values of α that are given above. The correct alias was selected at all but one point in the left track:

Figure 4.a. Processing details.

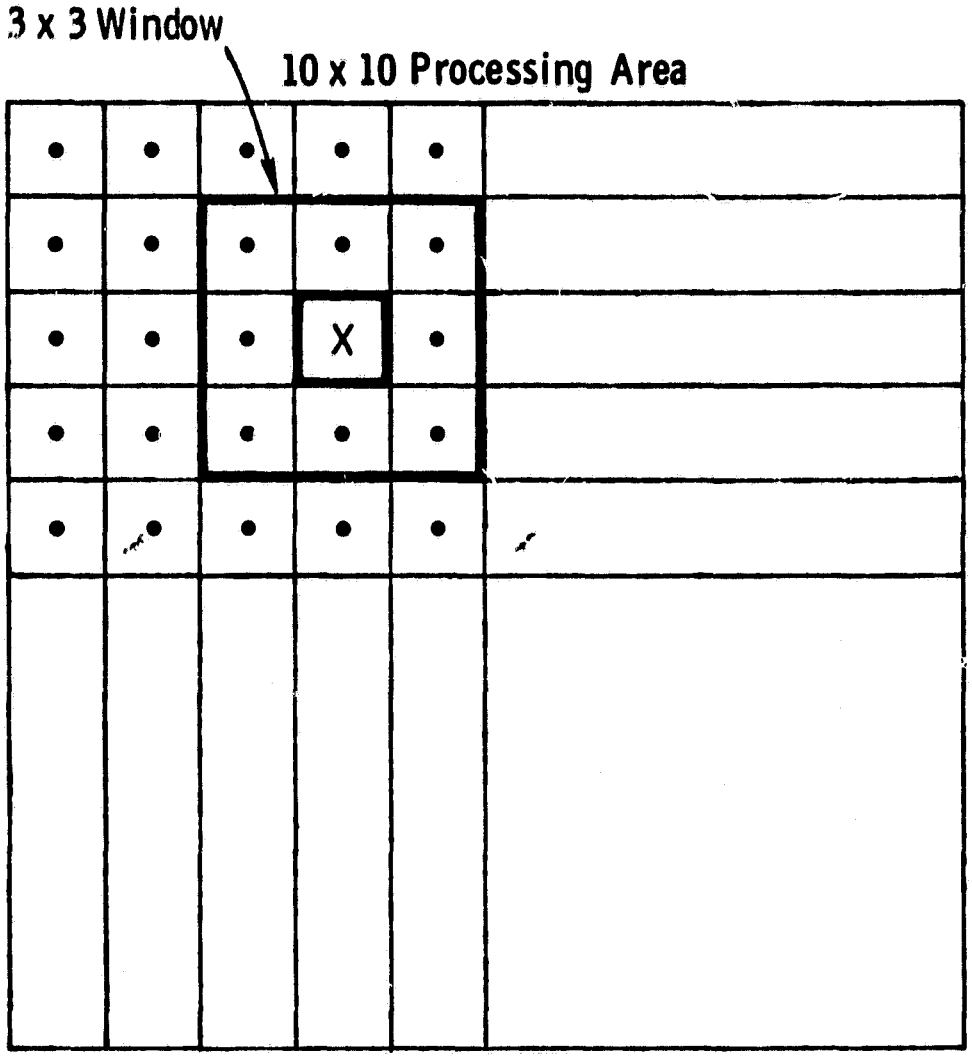

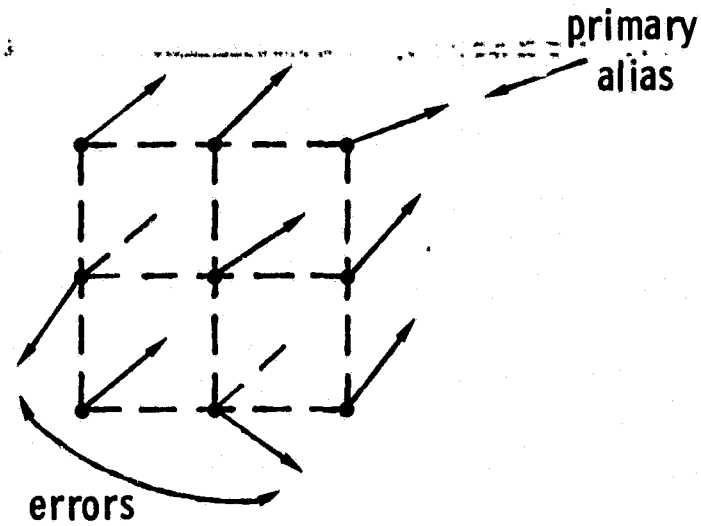

Total number of cells processed = 449

Number of times the primary alias
was closest to the true direction = 436 out of 449

Results of the alias removal
algorithms = 448 out of 449

The alias removal algorithm failed at one point, located at row 35, column 2. Detailed examination of Figure 4b shows that even though the alias removal algorithm failed at this point, the difference between the errors is small (8.7° compared to 31.3°).

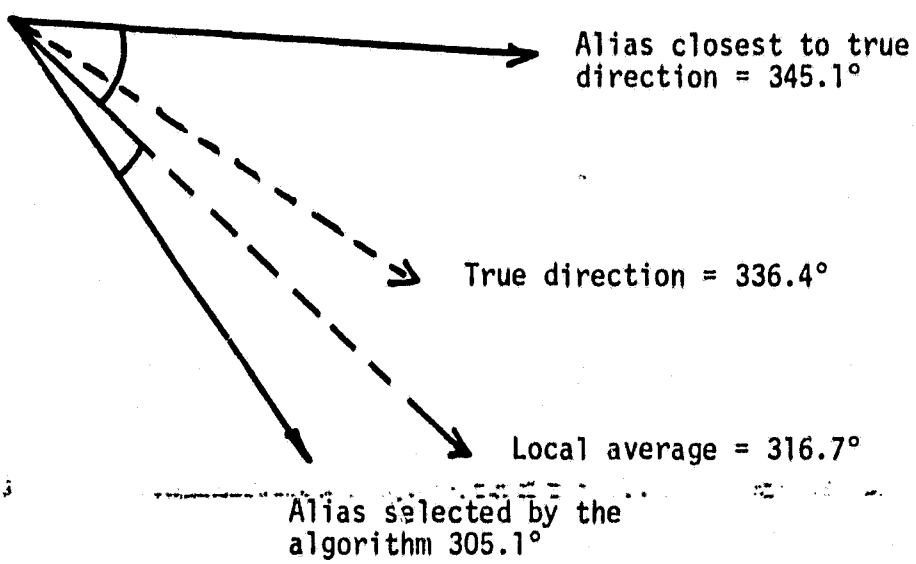

Figure 4.b. Alias directions at grid location (35,2), left track.

Instead of a 9 cell average, an 8 cell average could also be used, i.e., for each 3x3 window omit the center cell from mean and σ

calculations. Performance in this case was as good as in the 9 cell case.

The averaging algorithm was applied to a number of other tracks and the results are shown in Figures 5, 6 and 7. In Figures 6 and 7, the location of errors in the primary aliases (with the largest probability) and the location of errors after alias removal are explicitly shown. The results shown in Figures 5-7 indicate that the averaging algorithm indeed works very well, and the improvement in accuracy is of the order of 8-12%, from 86% prior to dealiasing to about 98% after alias removal.

Figure 5. Alias removal based on averages.

Rev: 0825, Left Track

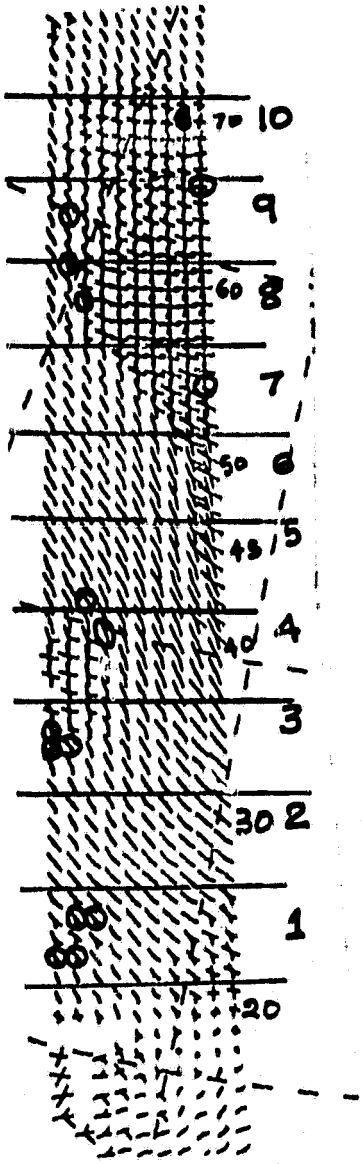

Location of Errors
Before Processing
Are Shown Circled

Total number of cells: 449

Number of errors in
the primary alias : 13

Number of errors
after processing : 1

Figure 6. Alias removal based on averages.

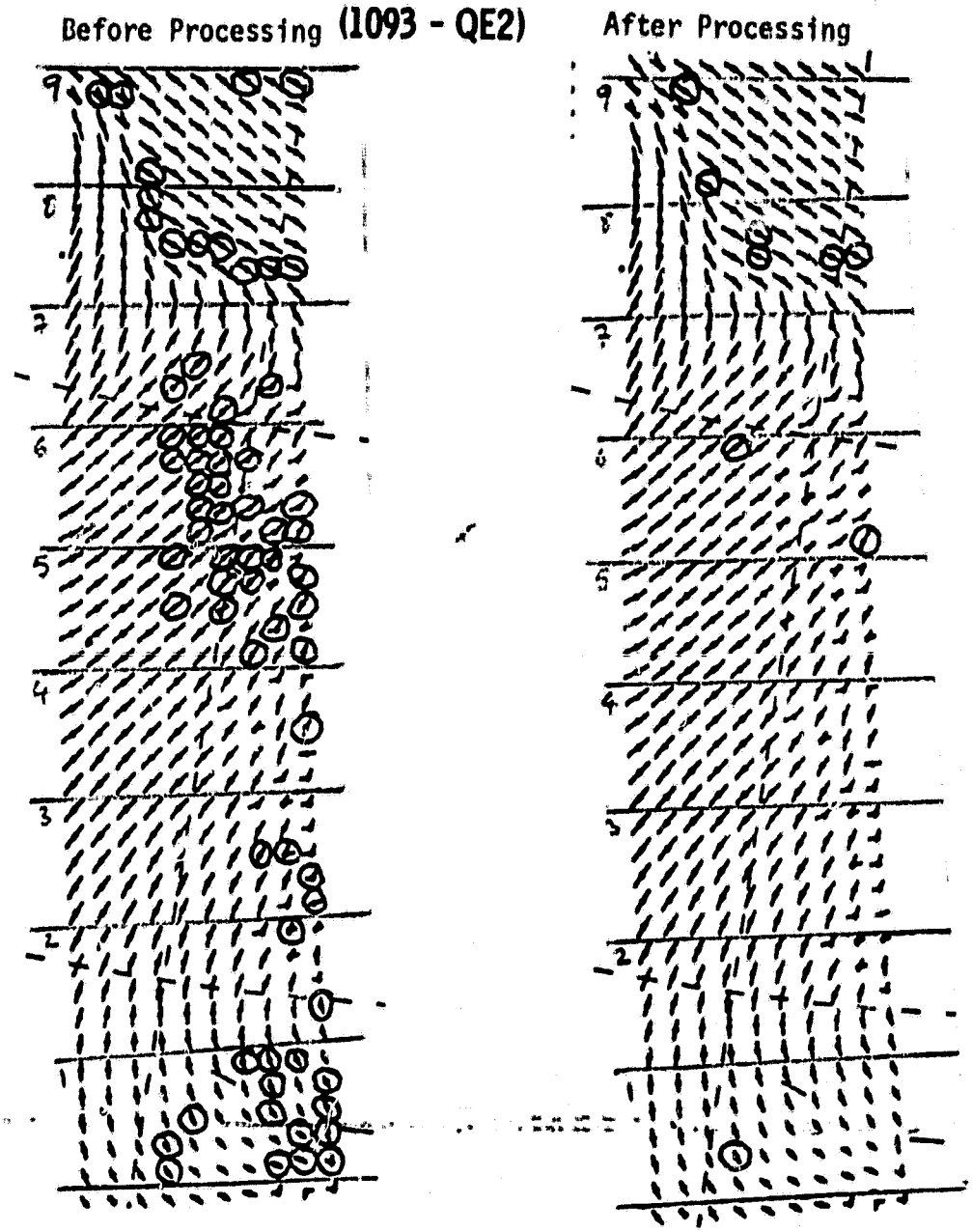

Total number of cells: 450

Number of errors in the primary alias : 68 (382/450)

Number of errors after processing : 9 (441/450)

(Location of Errors Are Shown Circled)

Figure 7. Alias removal based on averages.

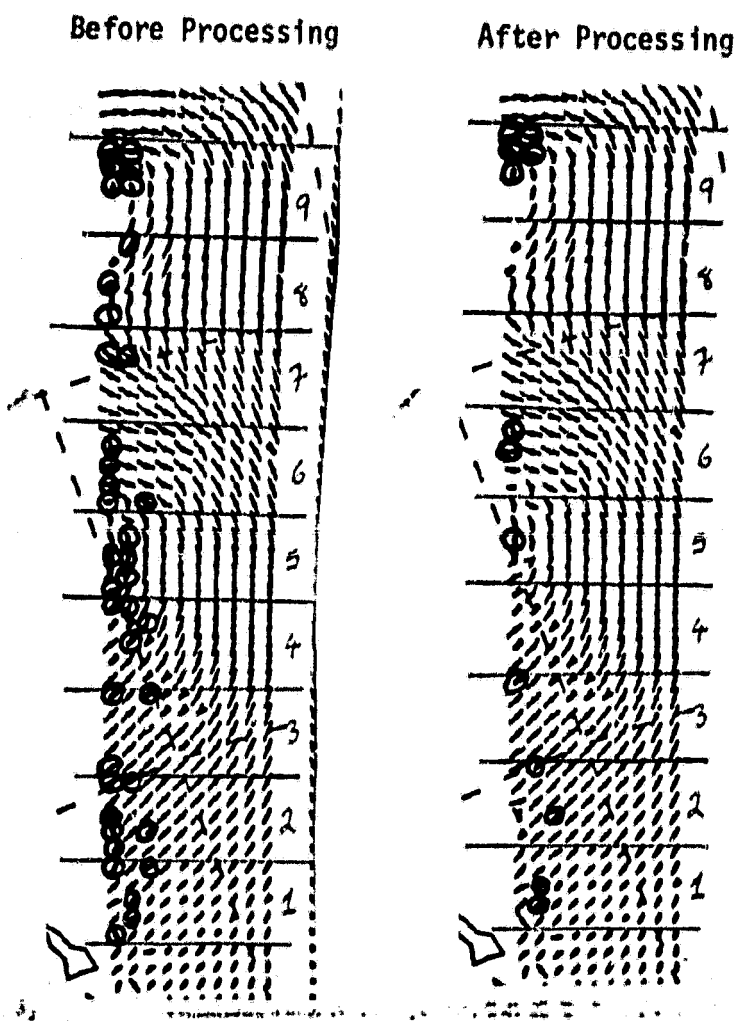

Total number of cells: 447

Number of errors in the primary alias : 39

Number of errors after processing : 13

(Location of Errors Are Shown Circled)

5.0 ALIAS REMOVAL BASED ON CURVE FITTING FOR STREAMLINES - RIGHT TRACK

The wind field over the right track area for Rev 0825 varies considerably. These variations are reflected in the values of the statistical parameters shown in Table 1.b (also see Figure 3.b). For example the wind direction has a mean standard deviation of 56° compared with 28° for the left track, and the entropy of the wind speed gradient is 1.79 compared to 0.74 for the left track. These variations indicate that an average based alias removal algorithm will not be successful and the structure of the streamline pattern within each processing area has to be taken into account by the alias removal algorithm. We focused our attention on blocks 5, 7 and 8 in the right track and used a curve fitting algorithm to find the best fit streamline pattern and use this pattern to aid in alias removal.

But, before proceeding to the streamline pattern analysis method, the entire right track was first processed using a 3x3 window and an 8 cell average. Next it was processed using a 9 cell average/global average with thresholding on $\alpha = 30°$. The results of these two operations are summarized in Table 2 (for blocks 5, 7, 8).

There is a deterioration in performance as we go from a simple 8 cell average to the thresholding case. The results in Table 2 indicate that the global mean can not be used for alias removal since it carries no information on the structure of a cyclonic vortex.

The curve fitting approach was considered next. In this approach, the streamline pattern in the vicinity of the low/cyclonic vortex was modeled by a set of concentric circles. This circular pattern was used to

Block #	Agreement Between Alias Closest to Average Direction and Alias Closest to True Direction		Agreements Between Alias Closest True Direction and Alias With Largest Probability
	8 Cell Avg.	9 Cell/Global Avg. With α = 30°	
5	35/47	25/47	33/47
7	38/46	26/46	36/46
8	45/50	41/50	45/50

Table 2

Results of Simple Local Averaging and Averaging With Threshold on Cyclonic Areas

predict the wind direction at any point. In the cyclonic vortexes of blocks 5, 7, 8 the flow is toward the center. This was incorporated by adding a constant 'inflow angle' to the direction predicted by the circular curve fitting. These angle calculations are summarized in Appendix III. Experiments were performed with various inflow angles and the results will be described later.

But at first in order to generate the circular pattern we need to locate the center of the cyclonic vortex. In order to do so we assume the center to be at a certain point. We then generate the wind directions at various points based on the circular pattern and find the error between these "circle fitted" directions and, say the true directions. The center is then moved to another point and the procedure is repeated. This generates a 3-dimensional map: location of center (row, column) versus rms error. Three such maps were generated:

(a) maps of rms error between true wind directions and "circle fitted" directions,

(b) alias direction closest to true direction and "circle fitted" directions,

(c) direction with largest alias probability and "circle fitted" directions (all with an inflow angle of 15°).

These three maps are shown in Tables 3.1, 3.2, 3.3 and 3.4.

The cell with the minimum rms error gives us the location of the center. Examining Tables 3.1, 3.2 we see that rms error increases as we go away from the center as would be expected. In Table 3.3, this behavior, though present is a bit erratic. Also, the locations of the center obtained from the three maps are different but adjacent to each other. In a real situation, only Table 3.3 would be available to the user. Using this table we can locate the cell with the minimum rms error and take this cell to be the center of the vortex. The streamline pattern corresponding to this center defines a unique, preferred wind direction at each grid location in the processing area.

The alias removal algorithm is now applied to each point in the processing area. A local mean and standard deviation are first calculated using 3x3 windows. If the local standard deviation is less than 30°, then the local average is taken to be the preferred direction. If not, the direction given by the streamline pattern is taken as the preferred direction. The alias closest to the preferred direction is selected as the estimate of the true wind direction. The alias probability is taken into account in the selection process as described in the previous section.

Several experiments were performed over blocks 5, 7, 8 in the right track to determine the sensitivity of the alias removal algorithm as a function of the location of the center of the low, and the inflow angle included, and the threshold on the local standard deviation. The performance of the alias removal algorithm was evaluated by counting

ROW \ COLUMN	17	18	19	20	21	22	23	24	25	26
48	86.86	78.52	70.77	64.52	62.57	63.19	68.13	73.47	78.3	78.9
47	84.22	75.1	66.42	57.19	53.43	53.93	38.5	63.91	69.45	73.03
46	82.43	72.47	62.16	52.0	45.11	44.92	48.86	55.48	62.73	69.35
45	82.31	72.33	61.45	50.25	40.63	37.84 (MIN)	42.36	50.36	58.60	66.49
44	83.17	73.62	63.35	52.96	43.38	39.38	43.89	50.71	58.44	66.44
43	85.93	77.62	68.51	59.23	51.68	48.3	48.76	54.28	61.28	68.08

Table 3.1

RMS Error Between "Circle Fitted" Directions
and True Wind Directions (Block #5)
(Inflow angle = 15°, α = 30°)

ROW \ COLUMN	17	18	19	20	21	22	23	24	25	26
48	86.7	78.3	70.53	64.65	63.73	63.89	68.51	74.81	81.15	82.95
47	83.79	76.35	64.69	56.9	55.08	55.09	60.05	66.86	72.99	77.32
46	82.04	71.25	60.2	50.12	46.18	46.15	52.02	59.42	67.11	72.83
45	81.53	70.95	59.07	47.1	39.96	40.04	45.75	54.47	63.03	71.0
44	81.83	71.69	60.43	50.62	40.53	39.02 (MIN)	46.42	54.6	61.9	69.77
43	83.67	76.29	65.48	55.93	48.29	46.42	50.88	57.16	62.79	70.55

Table 3.2

RMS Error Between "Circle Fitted" Directions
and Alias Closest to True Direction
(Inflow angle = 15°, α = 30°)

ROW \ COLUMN	17	18	19	20	21	22	23	24	25	26
48	95.96	89.10	82.7	77.46	75.12	7[illegible]5	76.38	77.05	77.52	79.75
47	93.49	85.92	78.29	71.80	68.56	[illegible]9.02	72.03	74.7	75.68	76.55
46	91.98	83.40	75.28	69.08	67.76	6[illegible].24	68.95	71.5	75.0	76.85
45	91.34	82.98	74.58	72.40	71.54	69.01	67.77	68.79	72.39	76.92
44	91.63	83.75	77.03	73.38	71.66	71.16	(MIN) 65.86	68.23	71.09	75.30
43	93.64	86.75	80.64	75.65	73.95	09.74	66.09	68.48	70.97	73.26

Table 3.3

RMS Error Between "Circle Fitted" Directions
and Direction with Largest Alias Probability for Block #5
(Inflow angle = 75°, α = 30°)

ROW \ COLUMN	17	18	19	20	21	22	23	24	25	26
60	101.24	92.3	82.51	72.37	62.87	55.57	51.78	48.77	51.39	56.5
59	98.21	88.95	78.82	68.39	58.74	54.47	48.75	(MIN) 46.73	48.4	53.32
58	96.05	86.95	77.01	66.67	61.9	54.23	50.38	48.41	48.53	51.33
57	94.31	85.78	76.7	67.93	61.57	58.28	53.14	47.4	50.09	50.26
56	92.77	85.34	77.8	70.54	66.03	59.11	54.71	50.01	50.66	52.56

Table 3.4

RMS Error Between "Circle Fitted" Directions
and Direction with Largest Alias Probability for Block #8
(Inflow angle = 0°, α = 30°)

the number of times the algorithm selected the alias closest to the true wind direction.

The results of the alias removal attempts on the right track are shown in Tables 4-7. These results, which correspond to $\beta = 0$ in Equation 1, indicate that the algorithms are fairly robust and show promise. As β was changed, the best results were obtained thus far with $\beta = 0.5$. In the vicinity of lows, the curve fitting approach selected the correct alias at 44 out of 47 points, and 89 out of 96 points. While the overall accuracy of 133 out of 143 points may be improved further, it is considerably better than the accuracy of the largest probability alias which is correct at only 114 out of 143 points.

Location of Center (JJJ,III)	RMS Error (From Table 3.3)	# of Agreements Between Alias Closest to 'Preferred' Direction and Alias Closest to True Direction	# of Agreements Between Alias Closest to True Direction and Alias Direction With Largest Probability
45,20	72.4	35/47	33/47
46,22	67.24	37/47	33/47
45,24	68.79	39/47	33/47
44,24	68.23	40/47	33/47
45,21	71.54	40/47	33/47
45,22	69.01	41/47	33/47
45,23	67.77	42/47	33/47
44,23	65.86 (MIN)	43/47	33/47

Table 4

Effect of Changing Center of Cyclone For Block #5
Algorithm Used: 9 cell average/"circle fit"
threshold on $\sigma = 30°$
inflow angle = 0°

Location of Center (JJJ,III)	RMS Error (From Table 3.4)	# of Agreements Between Alias Closest to 'Preferred' Direction and Alias Closest to True Direction	# of Agreements Between Alias Closest to True Direction and Alias Direction With Largest Probability
59,24	46.73 (MIN)	84/96	81/96
58,24	48.41	84/96	81/96
58,22	54.23	86/96	81/96

Table 5

Effect of Changing Center of Cyclone for Blocks 7 and 8
(Blocks 7 and 8 contain a single cyclonic vortex with the center somewhere in Block #8)
Algorithm Used: 9 cell average/"circle fit"
threshold on σ = 30°
inflow angle = 0°

Block #	Inflow Angle	# of Agreements Between Alias Closest To True Direction and Alias Closest to 'Preferred' Direction	# of Agreements Between Alias Closest To True Direction and Alias Direction With Largest Probability
5	0	43/47	33/47
5	5	43/47	33/47
5	15	44/47	33/47
5	20	44/47	33/47
5	25	44/47	33/47
5	45	38/47	33/47
7&8	0	86/96	81/96
7&8	15°	88/96	81/96

Table 6

Effect of Changing Inflow Angle

Value of Threshold (=σ)	# of Agreements Between Alias Closest To True Direction and Alias Closest to 'Preferred' Direction	# of Agreements Between Alias Closest To True Direction and Alias Direction With Largest Probability
60°	41/47	33/47
45°	42/47	33/47
30°	43/47	33/47
20°	43/47	33/47
15°	43/47	33/47
5°	43/47	33/47

Table 7

Effect of Changing Threshold Level For Block #5

Locations of errors before and after the alias removal algorithm was applied are shown in Figures 8, 9, and 10. Figure 10 displays a situation in the vicinity of a col-point to which the curve fitting (Appendix IV) approach was used with a good degree of success. While the averaging technique improves the accuracy of picking the correct solution from 85% to 95% and upwards, the curve fitting approach improves the accuracy from about 77% to 93% in the vicinity of singular points. Considering the large number of errors in the prime aliases near singular points, this improvement in accuracy is very significant.

Figure 8. Alias removal using curve fitting.

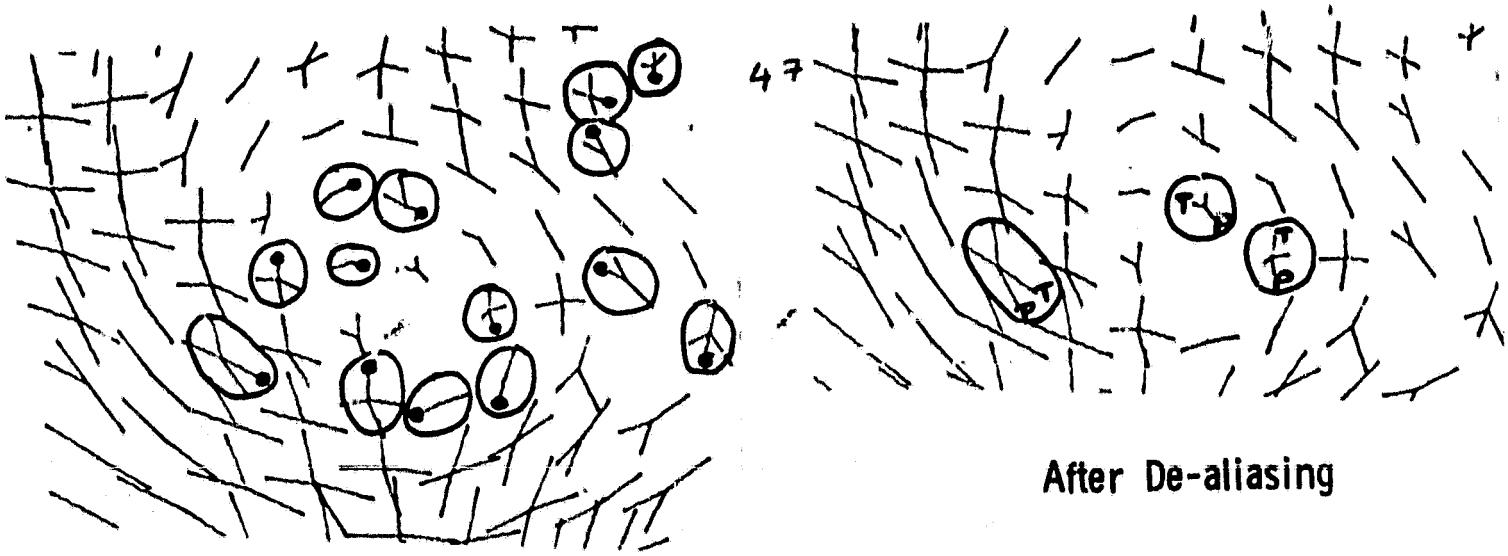

Before De-aliasing

After De-aliasing

Number of cells processed: 47

Number of errors in the primary alias : 14 (33/47)

Number of errors after processing : 3 (44/47)

Figure 9. Alias removal using curve fitting.

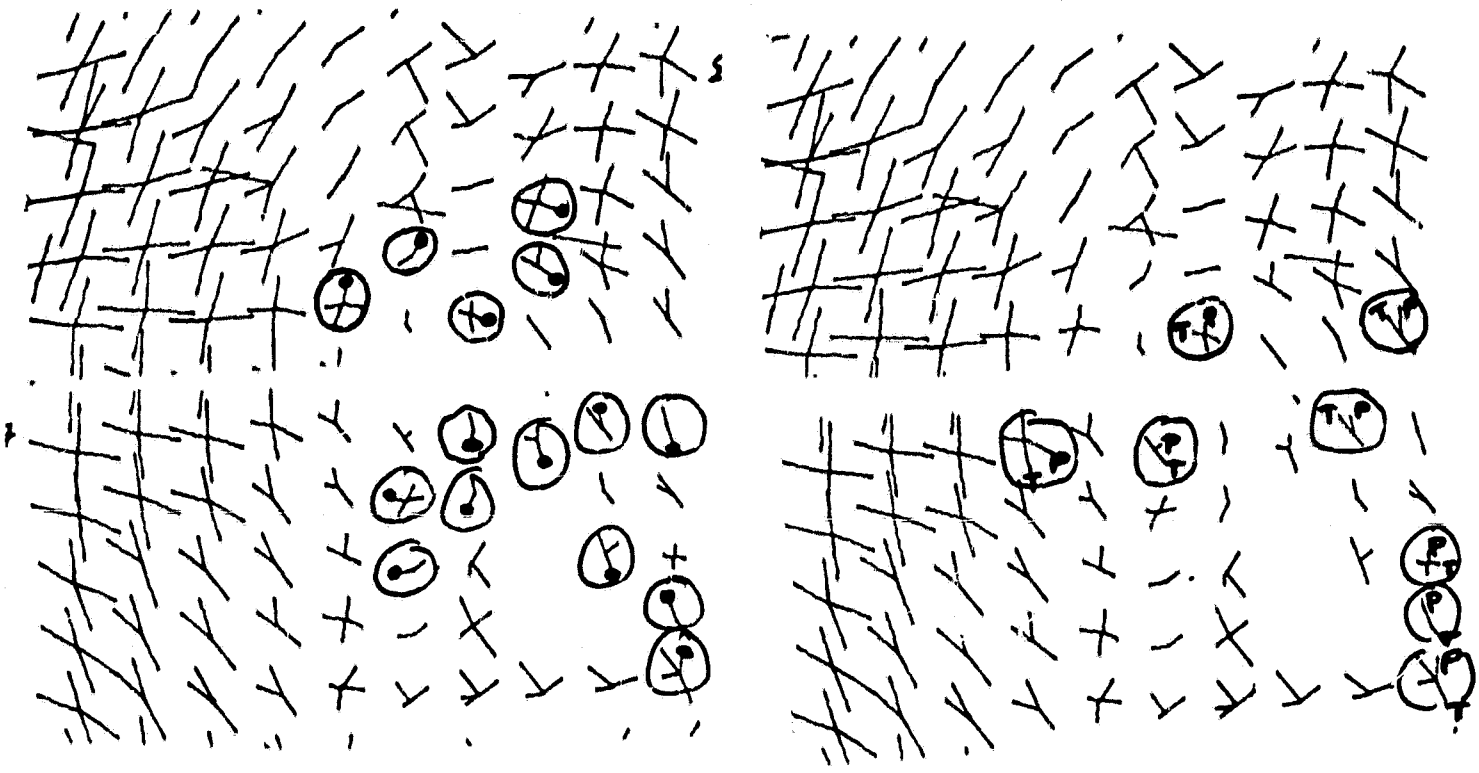

Location of Errors
Before De-aliasing

Location of Errors
After De-aliasing

Number of cells processed: 96

Number of errors in
the primary alias : 15 (81/96)

Number of errors
after processing : 8 (88/96)

Figure 10. Alias removal based on curve fitting, near a col-point.

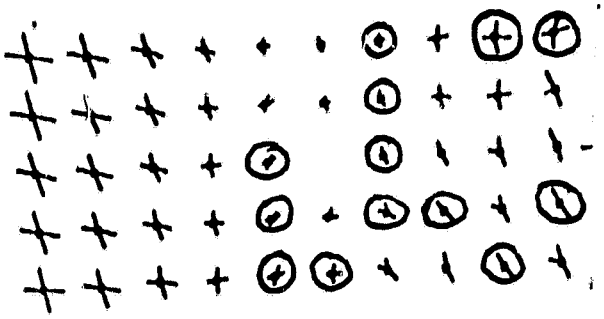

Errors in direction with largest alias probability

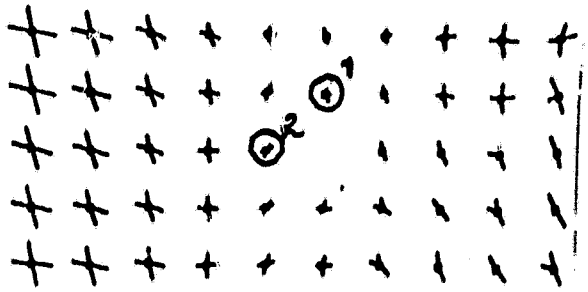

Location of errors after processing

6.0 CONCLUSIONS

We have presented in this report a set of algorithms that can be used for removing aliases in the multiple wind vector solutions produced from NOSS-type scatterometer data. The algorithms are based on histogram analysis, local averaging and curve fitting. The histogram analysis is used to determine the degree of homogeneity of the wind field defined by the largest probability alias vector at each grid point. Depending on the degree of homogeneity, either a local averaging technique or a curve fitting technique is used to find a "preferred" wind direction at each grid location. The alias directions are compared with the preferred direction at each grid location and one of the multiple aliases is chosen as the true direction based on its closeness to the preferred direction and its probability.

The alias removal algorithms were applied to a number of simulated NOSS-SCAT data sets. The alias removal algorithms produced correct wind vectors with an accuracy of over 95%. This compares with about 80 to 85% of the grid points at which the alias with the largest probability is also the correct solution.

Additional improvement in performance may be realized by combining our procedure with other algorithms. To help improve our performance near singular points and frontal zones, a catalog of histograms for various categories of streamline patterns should be developed.

Appendix I

Mean and Standard Deviation of Angles

(a) Compute Histogram

C_1	C_2		C_8	C_9			C_{16}
θ_1	θ_2	. . . . .	θ_8	θ_9	. . . . .		θ_{16}

22.5° 45° 180°

C_i = (weighted) count in the ith cell

θ_i = mid point of cell i; $\theta_i = 11.25° + (i-1)\ 22.5°$

(b) Compute two different means

$$\bar{\theta}_u = \sum_{i=1}^{8} C_i\theta_i \Big/ \sum_{i=1}^{8} C_i \quad \text{(mean of upper quadrants)}$$

$$\bar{\theta}_\ell = \sum_{i=9}^{16} C_i\theta_i \Big/ \sum_{i=9}^{16} C_i \quad \text{(mean of lower quadrants)}$$

Let $X_1 = \sum_{i=1}^{8} C_i$

$X_2 = \sum_{i=9}^{16} C_i$

(c) If $\bar{\theta}_\ell - \bar{\theta}_u < 180°$ $\qquad \bar{\theta} = \dfrac{\bar{\theta}_u X_1 + \bar{\theta}_u X_2}{X_1 + X_2}$

$\bar{\theta}_\ell - \bar{\theta}_u \geq 180°$ $\qquad \bar{\theta} = \dfrac{\bar{\theta}_u X_1 + (\bar{\theta}_\ell - 360) X_2}{X_1 + X_2}$

where $\bar{\theta}$ is the required mean.

(d) Variance = $$\frac{\sum_{i=1}^{16} d_i^2 C_i}{\sum_{i=1}^{16} C_i}$$

where $d_i = \min(|\theta_i - \bar{\theta}|, 360 - |\theta_i - \bar{\theta}|)$

Appendix II

Max Gradient

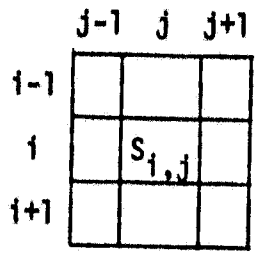

$S_{i,j}$ = average wind speed at location i,j.

To find the max gradient at location i,j the following four masks are used on the above window:

1	1	1
0	0	0
-1	-1	-1

0	1	1
-1	0	1
-1	-1	0

-1	0	1
-1	0	1
-1	0	1

-1	-1	0
-1	0	1
0	1	1

$$D_1 = (S_{i-1,j-1} + S_{i-1,j} + S_{i-1,j+1} - S_{i+1,j+1} - S_{i+1,j} - S_{i+1,j-1})/6$$

$$D_2 = (S_{i-1,j} + S_{i-1,j+1} + S_{i,j+1} - S_{i+1,j} - S_{i+1,j-1} - S_{i,j-1})/6$$

$$D_3 = (S_{i-1,j+1} + S_{i,j+1} + S_{i+1,j+1} - S_{i+1,j-1} - S_{i,j-1} - S_{i-1,j-1})/6$$

$$D_4 = (S_{i,j+1} + S_{i+1,j+1} + S_{i+1,j} - S_{i,j-1} - S_{i-1,j-1} - S_{i-1,j})/6$$

Max gradient at (i,j) = $MAX(|D_1|, |D_2|, |D_3|, |D_4|)$.

Appendix III

Modelling the Cyclonic Vortex as Concentric Circles

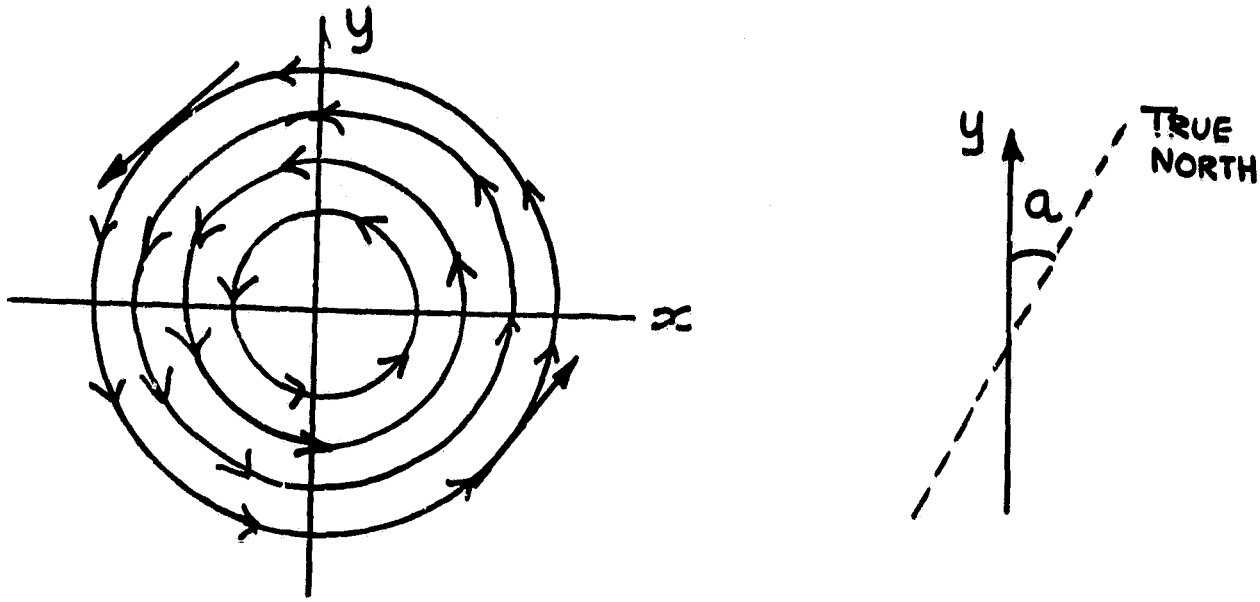

Figure III.a. Modelling the cyclonic vortex as concentric circles. (The true north is offset by a° from the perpendicular.)

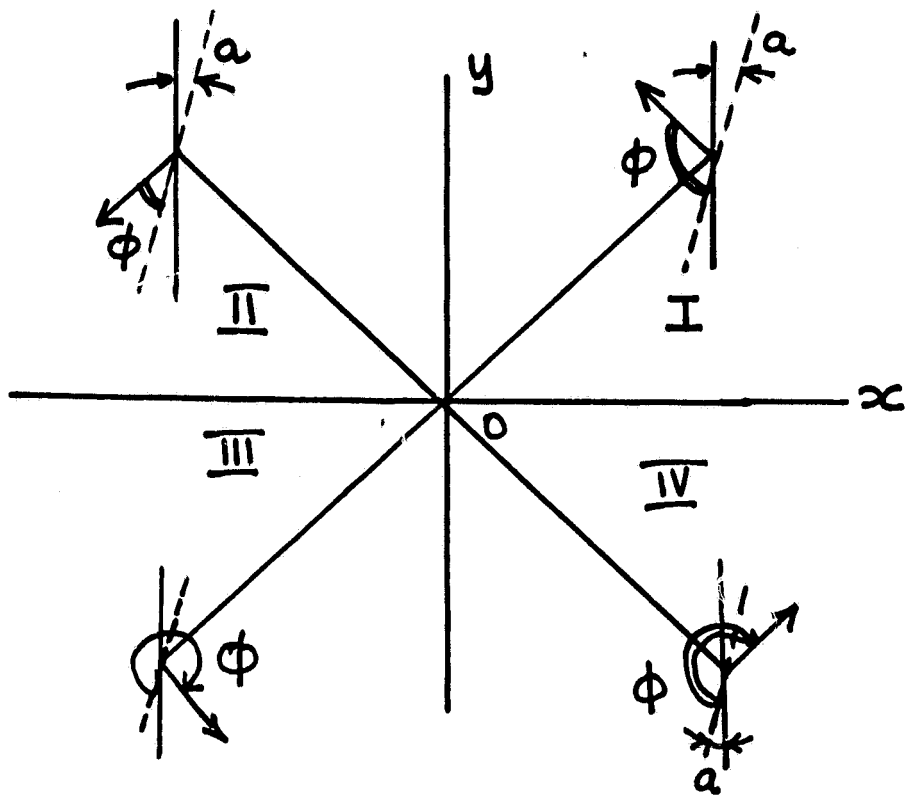

Figure III.b. Angle calculations in the various quadrants.

The center of the cyclone is assumed to be at (0,0)

$$\theta = \tan^{-1}\left(\frac{|y_1|}{|x_1|}\right)$$

ϕ is the required wind direction measured with respect to the true north. In Quadrant I: $\phi = 180 - \theta - a$

II: $\phi = \theta - a$

III: $\phi = 360 - \theta - a$

IV: $\phi = 180 + \theta - a$

To incorporate the inflow angle:

a ← a + inflow angle.

Appendix IV

Model For Col-Points

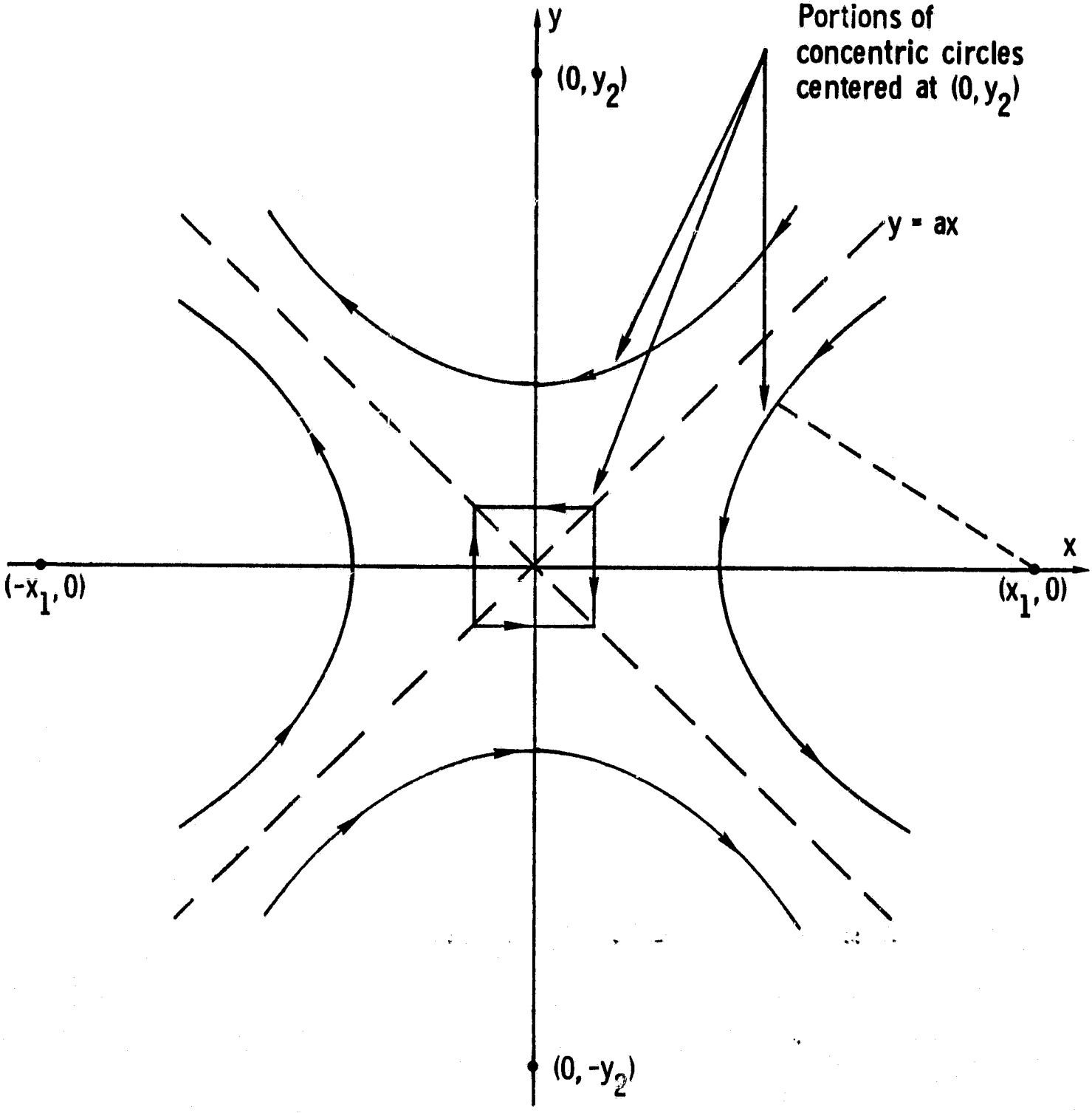

Figure IV.a. Curve-fitting model for col-points.